



# CHORUS

This is the accepted manuscript made available via CHORUS. The article has been published as:

## Revised analysis of $^{40}\text{Ca} + ^{96}\text{Zr}$ fusion reactions

H. Esbensen, G. Montagnoli, and A. M. Stefanini

Phys. Rev. C **93**, 034609 — Published 10 March 2016

DOI: [10.1103/PhysRevC.93.034609](https://doi.org/10.1103/PhysRevC.93.034609)

# Revised analysis of $^{40}\text{Ca}+^{96}\text{Zr}$ fusion reactions

H. Esbensen<sup>1</sup>, G. Montagnoli<sup>2</sup>, and A. M. Stefanini<sup>3</sup>

<sup>1</sup>*Physics Division, Argonne National Laboratory, Argonne, Illinois 60439*

<sup>2</sup>*Dipartimento di Fisica e Astronomia, Università di Padova,  
and INFN, Sez. di Padova, I-35131 Padova, Italy, and*

<sup>3</sup>*INFN Laboratori Nazionale di Legnaro, I-35020 Legnaro (Padova), Italy*

(Dated: February 19, 2016)

## Abstract

Fusion data for  $^{40}\text{Ca}+^{96}\text{Zr}$  are analyzed by coupled-channels calculations that are based on a standard Woods-Saxon potential and include couplings to multiphonon excitations and transfer channels. The couplings to multiphonon excitations are the same as used in a previous work. The transfer couplings are calibrated to reproduce the measured neutron transfer data. This type of calculation gives a poor fit to the fusion data. However, by multiplying the transfer couplings with a  $\sqrt{2}$  one obtains an excellent fit. The scaling of the transfer strengths is supposed to simulate the combined effect of neutron and proton transfer, and the calculated one- and two-nucleon transfer cross sections are indeed in reasonable agreement with the measured cross sections.

PACS numbers: 25.70.-z, 25.70.Hi, 25.70.Jj

## I. INTRODUCTION

In this work we try to explain the fusion data for  $^{40}\text{Ca}+^{96}\text{Zr}$  by coupled-channels calculations. The data were first measured by Timmers et al. [1] and they have been a challenge to theory for many years [2], primarily because they are strongly enhanced at subbarrier energies (see Fig. 1 of Ref. [3]) compared to the data for  $^{40}\text{Ca}+^{90}\text{Zr}$  [1] and the more recent data for  $^{48}\text{Ca}+^{90,96}\text{Zr}$  [4]. It has been suggested that the enhancement is caused by the influence of neutron transfer reactions because the ground state  $Q$  values for neutron transfer are positive for this system, whereas they are negative for the  $^{90}\text{Zr}$  target (see Table 4 of Ref. [1]). The expectation that the couplings to transfer channels with positive  $Q$  values could lead to an enhancement of subbarrier fusion was first proposed by Broglia et al. [5] in an attempt to explain the fusion data for the Ni+Ni isotopes [6].

We have previously tried to explain the fusion data for the Ca+Zr isotopes [1, 4] by coupled-channels calculations [7]. We found that the couplings to multiphonon excitations play a very important role in explaining the enhancement of the subbarrier fusion data. They appeared to be sufficient to account for the  $^{40}\text{Ca}+^{90}\text{Zr}$  data but they were clearly insufficient in explaining the  $^{40}\text{Ca}+^{96}\text{Zr}$  data. We tried to explain the latter data by introducing a strong coupling to two-neutron transfer reactions but the attempt was unsuccessful [7].

In order to better understand the influence of transfer on the fusion of  $^{40}\text{Ca}+^{96}\text{Zr}$ , the cross sections for one- and two-neutron transfer reactions were measured [8–10]. In this work we calibrate the one- and two-neutron transfer form factors so that the transfer data are reproduced by our coupled-channels calculations. We shall see that the subbarrier fusion is enhanced due to the couplings to the neutron transfer channels but the enhancement is not strong enough to explain the fusion data. A similar conclusion was recently reached by Scamps and Hagino [11]. In contrast, Sargsyan et al. [12] have claimed that the fusion data can be explained by considering the change in the deformation of the reacting nuclei after the two-neutron transfer has taken place.

We mentioned in our earlier work [7] that the effective ground state  $Q$  values for one- and two-proton transfer reactions are positive in  $^{40}\text{Ca}+^{96}\text{Zr}$  collisions. The couplings to these reaction channels could therefore also lead to an enhancement of the subbarrier fusion cross sections. A rough estimate of the combined effect of the couplings to the neutron and proton transfer channels is to multiply the neutron transfer couplings with a factor of  $\sqrt{2}$ . We shall

see that this simple estimate gives an excellent account of the fusion data. It also gives a fairly reasonable account of the measured one- and two-nucleon transfer cross sections, although a detailed comprehension of these data is outside the purpose of the present work.

The manuscript is organized as follows. The results of a previous analysis of the  $^{40}\text{Ca}+^{96}\text{Zr}$  fusion data, and the challenges that remain, are summarized in the next section. The model that is used to describe the influence of inelastic excitations and nucleon transfer reactions on heavy-ion fusion cross sections is reviewed in Sec. III. The sensitivity to multiphonon excitations and multinucleon transfer reactions is investigated in Sec. IV, and the conclusions are presented in Sec. V.

## II. SUMMARY OF PREVIOUS RESULTS

The formalism for the coupled-channels calculations we perform is described in detail, for example, in Sec. III of Ref. [2]. The formalism was applied in Ref. [7] to analyze the data for the fusion of the Ca+Zr isotopes [1, 4]. Most of the data were explained fairly well by considering multiphonon excitations with up to three-phonon excitations, and a relatively modest influence of nucleon transfer reactions. One exception was the fusion of  $^{40}\text{Ca}+^{96}\text{Zr}$  which could not be reproduced at subbarrier energies, even when a very strong pair-transfer coupling was applied.

Another interesting feature of the analysis for the Ca+Zr fusion data is that most of the data were best reproduced by applying the so-called M3Y+repulsion, double-folding potential [7]. Having determined the densities of the reacting nuclei it is possible to predict the ion-ion potential. It turned out that the ion-ion potential that could be predicted for  $^{40}\text{Ca}+^{96}\text{Zr}$  produced a Coulomb barrier that was much too high. The data were much better described by applying an ordinary Woods-Saxon (WS) potential, with a 1.5 MeV lower Coulomb barrier. Such a potential will therefore be applied in the following.

The  $^{40}\text{Ca}+^{90,96}\text{Zr}$  fusion data by Timmers et al. [1] are compared in Fig. 1 to coupled-channels calculations that are based on standard WS potentials of the proximity type described by Eqs. (III.40-41) and (III.44-45) in Ref. [14]. The parameters of the calculations and the channels that were included are discussed in detail in Ref. [7]. The data for  $^{40}\text{Ca}+^{96}\text{Zr}$  were recently supplemented with new measurements [13]. They are shown in Fig. 1 by the solid black diamonds and reach cross sections as small as 2.4  $\mu\text{b}$ .

The two Ch-1 calculations farthest to the right in Fig. 1 show the no-coupling limits for the two systems. The Ch-27 calculation for  $^{40}\text{Ca}+^{90}\text{Zr}$  (blue dashed curve) includes couplings of up to three-phonon excitations, with a total of 27 channels. The Ch-28 calculation for  $^{40}\text{Ca}+^{96}\text{Zr}$  is similar and has 28 channels (the green dashed curve). It is seen that the Ch-27 calculation reproduces the data for the  $^{90}\text{Zr}$  target quite well, whereas the Ch-28 calculation underpredicts the data for the  $^{96}\text{Zr}$  target at subbarrier energies. The qualitative reason for the difference in these results is (as mentioned in the introduction) that the ground state  $Q$  values for neutron transfer reactions are positive for the  $^{96}\text{Zr}$  target, whereas they are negative for the  $^{90}\text{Zr}$  target. The influence of transfer is therefore expected to play a major role in the fusion of  $^{40}\text{Ca}+^{96}\text{Zr}$ , and only a minor role in the fusion of  $^{40}\text{Ca}+^{90}\text{Zr}$ .

In an attempt to explain the  $^{40}\text{Ca}+^{96}\text{Zr}$  fusion data, the combined effect of multiphonon excitations and couplings to one- and two-neutron transfer reactions were included in Ref. [7] in Ch-84 calculations. The result is shown by the solid red curve in Fig. 1. The WS potential and the strength of the pair-transfer coupling were adjusted to optimized the fit to the high energy fusion data. This procedure failed and resulted in the discrepancy with the low-energy data that can be seen in Fig. 1. In the following sections we investigate what could be the reason for the failure.

### III. COUPLED-CHANNELS CALCULATIONS

The WS potential that was used previously for  $^{40}\text{Ca}+^{96}\text{Zr}$  [7] is adopted here for simplicity. It has the parameters  $R = 9.599$  fm,  $V_0 = -73.98$  MeV, and diffuseness  $a = 0.673$  fm. The total potential for angular momentum  $L = 0$  has a Coulomb barrier height of 96.62 MeV and a pocket of 73.62 MeV. The pocket is safely above the ground state energy of the  $^{136}\text{Nd}$  compound nucleus which is  $E_{CN} = 41.089$  MeV.

We also use the same one-, two-, and three-phonon excitations that were used in Ref. [7]. The calculation with one- and two-phonon excitations has 18 channels and is referred to as the Ch-18 calculation. The calculation with up to three-phonon excitations has 28 channels and is called the Ch-28 calculation.

The influence of transfer is modeled as first described in Ref. [15]. The model has since been used in several publications, including the study of multineutron transfer reactions in  $^{58}\text{Ni}+^{124}\text{Sn}$  collisions [16] and our recent work on the fusion of Ca+Zr isotopes [7]. Since the

calculations failed to reproduce the fusion data for  $^{40}\text{Ca}+^{96}\text{Zr}$ , we repeat them here with a careful calibration of the couplings to transfer channels. The basic ingredients of the model are summarized below.

### A. Model of neutron transfer

One complication in coupled-channels calculations of transfer reactions is the enormous number of channels that exist. The calculations can be simplified by adopting the rotating frame approximation [2] which is commonly used in coupled-channels calculations of fusion reactions. The number of transfer channels is reduced further by lumping them together to only one effective channel for each mass partition. The basic calculation includes zero-, one-, two- and the three-neutron transfer channels. Without any influence of inelastic excitations, it consists of 4 channels and is denoted the Ch-4 calculation.

The effective form factor for one-neutron transfer is first constructed from the transfer of the fully occupied  $d_{5/2}$  and  $s_{1/2}$  states in  $^{96}\text{Zr}$  to the unoccupied  $f_{7/2}$  state in  $^{41}\text{Ca}$  as described in Refs. [15] using the so-called Quesada form factors [17]. This effective form factor is denoted  $f_{1n}^{\text{eff}}(r)$ . The coupling  $\langle 1n|V|0n\rangle$  of the zero- and the one-neutron transfer channels is assumed to be proportional to  $f_{1n}^{\text{eff}}(r)$ ,

$$\langle 1n|V|0n\rangle = F_{1n} f_{1n}^{\text{eff}}(r), \quad (1)$$

where the strength  $F_{1n}$  is adjusted so that the one-neutron transfer data are reproduced. The reason for this calibration is that it is very difficult to make a good absolute prediction of the one-neutron transfer cross section.

The couplings between the successive one-neutron transfer channels are also constructed by simple scaling of the form factor  $f_{1n}^{\text{eff}}(r)$ . The scaling factors that are used are motivated by the systematics of transfer reactions that was observed in Ref. [18]. The basic observation was that the Q value distribution for transfer reactions is a Gaussian that is centered at the optimum Q value, which is of the order of +1 MeV. The distribution has a maximum cutoff which is the Q value for the ground state to ground state transition.

The effective ground state Q value for the first one-neutron transfer is 0.61 MeV [7]. This means that only about half of the Gaussian Q value distribution is accessible because the optimum Q value is close to +1 MeV. The ground state Q value for two-neutron transfer is

$Q_{2n} = +5.52$  MeV [7]. This implies that the full Gaussian  $Q$  value distribution is accessible to the second one-neutron transfer. The coupling between the one-neutron and the two-neutron transfer channels is therefore estimated by

$$\langle 2n|V|1n\rangle = \sqrt{2} F_{1n} f_{1n}^{\text{eff}}(r). \quad (2)$$

All of the two-neutron transfer channels are lumped together in the coupled-channels calculations into one effective channel and the  $Q$  value of this channel is set to +1 MeV.

The coupling between the two- and three-neutron transfer channels is set to

$$\langle 3n|V|2n\rangle = \sqrt{3/2} F_{1n} f_{1n}^{\text{eff}}(r). \quad (3)$$

The  $Q$  value for the ground state to ground state three-neutron transfer is also large and positive ( $Q_{3n} = +5.24$  MeV), and one would therefore expect a scaling factor between 1 and the  $\sqrt{2}$  in Eq. 3. The factor was set to the  $\sqrt{3/2}$  in Refs. [15, 16] and that value is also adopted here. The effective  $Q$  value for the three-neutron transfer is set to +1 MeV in the coupled-channels calculations.

The model described above is calibrated so that the measured one-neutron transfer probabilities of Ref. [10] are reproduced for large values of the minimum distance  $D$  between the reacting nuclei. The strength that is required to reproduce the data in Ch-4 calculations is  $F_{1n} = 1.6$  and the results are shown in Fig. 2. It is seen that the two-neutron transfer probabilities are under-predicted by the successive Ch-4 calculation (the green dashed curve).

In order to reproduce the two-neutron data shown in Fig. 2, we supplemented the transfer couplings described above with the simple pair-transfer coupling originally introduced by Dasso and Pollarolo [19],

$$\langle 2n|V|0n\rangle = -F_{2n} \frac{dU(r)}{dr}, \quad (4)$$

where  $U(r)$  is the nuclear potential. In calculations with up to three-neutron transfers we use the same expression, Eq. (4), for the coupling between the one-neutron and three-neutron transfer channels. The measured two-neutron transfer probabilities shown in Fig. 2 are reproduced quite well at large values of  $D$  by choosing the pair-transfer strength  $F_{2n} = 0.25$  fm. The result is shown by the solid (red) curves. It is seen that the calculated one-neutron transfer probabilities are not much affected by the pair-transfer coupling, except for  $D \leq 13$  fm.

## B. Combined effect of excitations and transfer

The basic assumption of the model developed in Refs. [15, 16] is that inelastic excitations and the neutron transfer are independent degrees of freedom. In order to simplify the model it is therefore assumed that the excitation spectrum is the same in all of the mass partitions that are considered. This implies that if we use the 28 excitation channels mentioned earlier and combine them with up to three-neutron transfers, the full calculation will have  $4 \times 28 = 112$  channels (Ch-112). If we only include up to two-nucleon transfers, there will be  $3 \times 28 = 84$  channels (Ch-84).

The Ch-84 calculations that were performed in Ref. [7] are repeated here using the one- and two-neutron transfer strengths,  $F_{1n} = 1.6$  and  $F_{2n} = 0.25$  fm, that were calibrated in Ch-4 calculations to reproduce the measured one- and two-neutron transfer probabilities. The results of the Ch-84 calculations are shown by the black dashed curves in Fig. 2. It is seen that the transfer probabilities are insensitive to the excitations at minimum distances larger than 13 fm because they are essentially identical to the results of the Ch-4 calculation shown by the solid red curves. The results are different at smaller minimum distances where fusion can occur and where coupled-channels effects are large.

The fusion cross sections that are obtained in the new Ch-84 calculations described above are shown by the solid red curves in Fig. 3(a) and (b). It is seen that the Ch-84 calculation does not reproduce the data at low energies (Fig. 3(a)), and it is slightly above the data at high energies (Fig. 3(b)). Assuming that the Ch-28 model of multiphonon excitations is realistic, it appears that the additional couplings to the one- and two-neutron transfer channels cannot explain the discrepancy with the measured fusion cross sections. A similar conclusion was recently reached by Scamps and Hagino [11] who also calibrated their transfer couplings to reproduce the neutron transfer data shown in Fig. 2 but underestimated the fusion cross sections at subbarrier energies (see Fig. 11 of Ref. [11].) We must therefore seek a different explanation for the discrepancy between theory and experiment. Sargsyan et al. suggested that the deformation of the reacting nuclei after the two-neutron transfer could explain the data [12]. However, they did not test the consistency of their model by comparing their calculations to the transfer data. We present in the next section what we believe to be a natural and consistent explanation, namely, that one should also consider the effect of couplings to one- and two-proton transfer channels.

### C. Adjusting the transfer strength.

The discrepancy in Figs. 3(a) and 3(b) between the Ch-84 calculation and the data can be reduced by increasing the transfer strengths. This is clear because a stronger transfer coupling will enhance the fusion cross sections at low energies, and it will reduce it at high energies. Both features are evidently needed according to the solid red curves in Figs. 3(a) and 3(b). One motivation for increasing the transfer strengths is that the effective ground state  $Q$  values for the one- and two-proton transfers are positive according to Table III of Ref. [7] and couplings to these reaction channels could therefore have a significant influence on fusion. Another motivation is that the fusion data for  $^{40}\text{Ca}+^{96}\text{Zr}$  and other heavy-ion systems were reproduced quite successfully by Pollarolo and Winther in applications of their semiclassical method [20]. The method includes the combined effects of surface excitations and nucleon transfer reactions, and it is likely that the success of the applications relied on the inclusion of both neutron and proton transfer.

We show in Figs. 4(a) and 4(b) a revised Ch-84 calculation in which the transfer coupling strengths were multiplied by a factor of  $\sqrt{2}$ , so that  $F_{1n} = 2.25$  and  $F_{2n} = 0.355$  fm. This simple scaling is a crude way of simulating the combined effect of couplings to neutron and proton transfer channels. It is seen that the revised Ch-84 calculation reproduce the data very well, both at low and at high energies. In fact, the average  $\chi^2$  is only 0.87, assuming a systematic error of 7%. The fit is much better than obtained in Fig. 1 with the old Ch-84 calculation of Ref. [7], and with the new calibrated Ch-84 calculation that is shown in Figs. 3(a) and (b).

The average  $\chi^2$  is shown in Table I for each of the three Ch-84 calculations discussed so far. The energy shift  $\Delta E$  that optimizes the fit of each calculation is also shown, together with the optimum  $\chi^2$ . The non-zero values of the energy shifts  $\Delta E$  reflect that the WS potential has not been adjusted in each case to minimize the  $\chi^2$ . For example, the optimum fit of the revised Ch-84 calculation is achieved by applying the energy shift  $\Delta E = -0.15$  MeV to the calculated cross section. The shift is equivalent to increasing the radius of the WS well by only 0.02 fm.

It is very interesting that we were not able to reproduce the fusion data in the old analysis of Ref. [7], where the assumed one-neutron transfer coupling was weak ( $F_{1n}=1$ ) and the two-neutron pair-transfer coupling was adjusted freely ( $F_{2n}=0.5$  fm). In contrast,

the new calculations shown in Figs. 4 and 5 reproduce the data surprisingly well. They use a much stronger one-nucleon transfer strength ( $F_{1n}=2.25$ ) and a weaker pair-transfer strength ( $F_{2n}=0.355$  fm). These results demonstrate that the calculated fusion cross sections are sensitive not only to the pair-transfer coupling but also to the successive one-nucleon transfer mechanism.

While the couplings to one-nucleon transfer reactions can be calibrated or tested against transfer data, as it was done in Fig. 2 for the neutron transfer, the couplings to the successive transfers described by Eqs. (2) and (3) are uncertain or model dependent. This introduces some uncertainty in the strength of the direct pair-transfer, which in this work is described by Eq. (4) and is calibrated so that the combined effect of the successive transfer and the direct pair-transfer reproduces the measured two-neutron transfer data. This uncertainty was also discussed in Ref. [11] and needs to be resolved in the future.

Although the revised Ch-84 calculation shown in Fig. 4 is in remarkably good agreement with the data, it is useful to study the sensitivity to the multiphonon excitations and to the number of transfer channels because the parameters for these reaction channels are uncertain. The good agreement with the fusion data could therefore be accidental.

#### IV. DEPENDENCE ON MULTIPHONON EXCITATIONS AND TRANSFER

It is of interest to study the sensitivity of the calculated fusion cross sections both to number of multiphonon excitations and to the number of nucleon transfers that are considered. Ideally one would expect that the most complete calculation in terms of multiphonon excitations and nucleon transfer channels would provide the best fit to the fusion data. However, that may not be true in practice because of the approximations and model assumptions that have been made.

It is also important to test the consistency of the calculated fusion and transfer cross sections and to see if the calculation that provides the best fit to the fusion data can also account for the total one- and two-nucleon transfer cross sections that have been measured [8]. All of the calculations that are presented in this section are based on the WS potential that was described in the beginning of section III. The calculations that include couplings to transfer channels will be based on the revised transfer strengths:  $F_{1n} = 2.25$  and  $F_{2n} = 0.355$  fm that were proposed in subsection III.C.

The most obvious way to judge the qualities of the fits to the fusion data is to compare the  $\chi^2/N$ . Another way is to compare the barrier distributions obtained from the calculations and the data. It turns out that the calculated distributions are sensitive to multiphonon excitations and to the transfer couplings, and a comparison of the experimental barrier distribution may therefore help us identify the features that are missing in the calculations.

### A. Fusion cross sections

The calculated fusion cross sections are shown in Fig. 5. The coupled-channels calculations shown in Fig. 5(a) are all based on the Ch-18 calculation that includes couplings to one- and two-phonon excitations. The Ch-54 calculation has up to two-nucleon transfers, whereas the Ch-72 calculation includes up to three-nucleon transfers as explained in subsection II.B. It is seen that the Ch-72 calculation gives the better fit to the fusion data, both at low energies and overall in terms of the  $\chi^2/N$  that is shown in Table I.

The coupled-channels calculations shown in Fig. 5(b) are based on the Ch-28 calculation that includes couplings of up to three-phonon excitations. It is seen that the Ch-84 and Ch-112 calculations provide better fits to the fusion data than do the Ch-54 and Ch-72 calculation that are shown in Fig. 5(a). This implies that multiphonon excitations play a very important role in producing a good fit to the data. The same conclusion was reached in Ref. [7] for the fusion of the other Ca+Zr systems.

The  $\chi^2/N$  for the different calculations are compared in Table I. The values confirm that the calculated fusion cross sections are sensitive to both multiphonon excitations and to the three-nucleon transfer. The fact that the Ch-84 calculation and not the Ch-112 calculation gives the smallest  $\chi^2/N$  is unfortunate and seems to contradict the expectation that the most complete calculation should provide the best fit to the data. This unfortunate result may be the consequence of the approximations and model assumptions we have made. For example, the proton and neutron transfer couplings were assumed to be similar and their combined effect was estimated by multiplying the neutron transfer couplings with a  $\sqrt{2}$ . This estimate may be too crude. In future work it would be desirable also to have detailed experimental information about the proton transfer reactions, so that one can treat the couplings proton transfer channels explicitly and calibrate their strengths to data.

## B. Two-nucleon transfer cross sections

The one- and two-nucleon transfer cross sections measured at two energies [8] are shown both in Fig. 5(a) and (b). They are compared to the calculations where the thinner curves indicate the results of the Ch-54 and Ch-84 calculations in (a) and (b), and the thicker curves show the results of Ch-72 and Ch-112 calculations in (a) and (b), respectively.

It is seen in Fig. 5(a) that the Ch-72 calculation, which provides the better fit to the fusion data, also gives the better fit to the measured one- and two-nucleon transfer cross sections. The situation is different in Fig. Fig. 5(b) where the Ch-84 calculation gives the better fit to the fusion data whereas the Ch-112 is in better agreement with the two-nucleon transfer data. In both cases it is the larger calculation that provides the better agreement with the transfer data. This conclusion implies that it is important to consider three-nucleon transfer reactions if one wants to develop a realistic description of the two-nucleon cross section.

The measured one- and two-nucleon cross sections are compared to the calculated cross sections in Table II. It is seen that the three-nucleon transfer reactions in the Ch-72 and Ch-112 calculations play an important role in improving the agreement with the data. The influence of multiphonon excitations is less important. This can be seen by comparing the results of the Ch-54 and Ch-84 calculations as well as the Ch-72 and Ch-112 calculations. Overall, the Ch-112 calculation is in fairly reasonable agreement with the measured cross sections, except at the lowest energy where the calculated two-nucleon transfer cross section is about twice the measured value.

## C. Barrier distributions

Another way of illustrating the sensitivity of the calculated fusion cross section to multiphonon excitations and transfer reactions is to plot the derivatives of the cross sections multiplied with the center-of-mass energy. The barrier distribution, for example, is defined as the second derivative [21]

$$B(E_{c.m.}) = \frac{d^2(E_{c.m.}\sigma_f)}{dE_{c.m.}^2}, \quad (5)$$

and it is illustrated in Figs. 6(a) and (b) for the six coupled-channels calculations that are shown in Fig. 5. The height of the Coulomb barrier in the entrance channel potential is indicated by the solid triangle. The calculations show that the couplings to multiphonon

excitations and transfer channels are both very important in reproducing the shape of the measured barrier distribution. The distributions shown here were calculated using the finite difference method and an energy step of  $\Delta E = 2$  MeV.

From the comparison of the measured and calculated barrier distributions shown in Fig. 6(a) and (b) it is clear that the Ch-84 and Ch-112 calculations produce the best shapes in comparison to the data. This indicates that multiphonon excitations play a very important role in reproducing the shape of the measured distribution. The influence of the couplings to transfer reactions is also important but the influence of the couplings to the three-nucleon transfer channels is modest. It has the effect of smoothing out certain structures in the barrier distribution. This can be seen by comparing the barrier distributions of the Ch-84 and Ch-112 calculations. It is seen that the Ch-84 distribution has two peaks at energies below the nominal Coulomb barrier, whereas the Ch-112 calculation has essentially only one very broad peak.

We saw earlier that the Ch-84 calculation gives the best  $\chi^2$  fit to the fusion data, whereas the Ch-112 calculation gives the best agreement with the transfer data. From the comparison of the measured and calculated barrier distributions it is not so clear which of the two calculations gives the best description of the data. A somewhat disturbing feature is that the measured distribution has three peaks below 100 MeV, whereas the calculations produce at most two peaks. It is not clear at the moment which reaction mechanism would produce the third peak of the measured distribution.

#### D. $S$ factor for fusion

One way to emphasize the behavior of the fusion cross section at low energies is to plot the  $S$  factor for fusion. It is here defined with respect to a reference energy  $E_{\text{ref}}$  as follows,

$$S(E_{c.m.}) = E_{c.m.} \sigma_f \exp(2\pi[\eta(E_{c.m.}) - \eta(E_{\text{ref}})]), \quad (6)$$

where  $\eta(E)$  is the Sommerfeld parameter. The results based on Ch-28 calculations are shown in Fig. 7. It is seen that some of the calculated  $S$  factors exhibit oscillations at the lowest energies. The oscillations are sensitive to the depth of the pocket in the entrance channel potential and their amplitude can be reduced by choosing a deeper pocket. The fact that the  $S$  factors obtained from the data do not show any sign of an oscillation at the lowest

energies may indicate that the pocket in the entrance channel potential is fairly deep.

The most impressive feature of Fig. 7 is the enormous enhancement of the calculated  $S$  factors with increasing number of channels when compared to the Ch-1 no-coupling calculation. Another interesting feature is that the data can be reproduced fairly well by calculations that use a standard WS potential with a diffuseness of  $a = 0.673$  fm. There is therefore not any sign of a fusion hindrance at the lowest energies, at variance with what has been observed in the fusion of other heavy-ion systems [2]. The classic example is the fusion of  $^{60}\text{Ni}+^{89}\text{Y}$  [22] where the data are strongly suppressed at low energies compared to coupled-channels calculations that are based on a standard WS potential. The hindrance has in some systems been so strong that the  $S$  factor developed a maximum. This is clearly not the case in Fig. 7.

The lack of hindrance in the  $^{40}\text{Ca}+^{96}\text{Zr}$  fusion data should be seen in contrast, for example, to the analysis of the  $^{48}\text{Ca}+^{96}\text{Zr}$  fusion data [4] which showed a clear sign of a hindrance at the lowest energies [23]. The lack of hindrance in the fusion of  $^{40}\text{Ca}+^{96}\text{Zr}$  correlates with the absence of Pauli blocking in transfer reactions near the optimum  $Q$  value, which is a consequence of the positive  $Q$  values for transfer. The hindrance in the fusion of  $^{48}\text{Ca}+^{96}\text{Zr}$ , on the other hand, correlates with negative transfer  $Q$  values and therefore with a Pauli blocking of transfer reactions near the optimum  $Q$  value.

## V. CONCLUSIONS

In this work we applied and tested a model of heavy-ion fusion and transfer reactions that is based on the coupled-channels approach. The basic assumption is that excitations and nucleon transfers are independent degrees of freedom. In the application of the model it is assumed that the excitation spectrum is the same in all of the mass partitions that are considered.

We applied the model to the fusion of  $^{40}\text{Ca}+^{96}\text{Zr}$  which is known to be very sensitive to the couplings to multiphonon excitations and transfer reactions. We first calibrated the transfer couplings so that the measured one- and two-neutron transfer probabilities were reproduced at large values of the minimum distance between projectile and target. We showed that the calculation that includes couplings to these transfer channels, as well as to multiphonon excitations with up to three-phonon excitations, cannot explain the fusion data

but underestimates them substantially at low energies. A similar conclusion was reached in a recent work by Scamps and Hagino [11].

In order to explain the fusion data we proposed to increase the strength of the transfer couplings. Such an increase is justified because the effective  $Q$  values for one- and two-proton transfers are positive and couplings to these reaction channels should therefore have an effect on fusion and enhance it at subbarrier energies. We assumed for simplicity that the neutron and proton transfers have similar effects on fusion and simulated their combined effect by multiplying the neutron transfer couplings with a factor of the  $\sqrt{2}$ . This estimate, combined with the influence of multiphonon excitations, turned out to produce a fusion cross section that is in remarkably good agreement with the data. Moreover, the predicted transfer cross sections are in fair agreement with the measured one- and two-nucleon transfer cross sections.

It is very interesting that we were not able to explain the  $^{40}\text{Ca}+^{96}\text{Zr}$  fusion data in a previous work [7], where the pair transfer strength was adjusted freely in similar coupled-channels calculations, without constraining the calculations by transfer data. The reason this approach failed must be that the assumed single-particle transfer strength was too small.

In future work it would be desirable to measure the neutron and the proton transfer cross sections in greater detail, as well as the cross sections for other reactions with small or positive  $Q$  values. It would, in particular, be useful to generalize the model we have used and treat explicitly the neutron and proton transfer channels, as well as other reaction channels that could have an influence on fusion. Such a generalization looks very promising in view of the present work. It should be feasible and fairly straightforward.

**Acknowledgments.** H. E. was supported by the U.S. Department of Energy, Office of Science, Office of Nuclear Physics, Contract No. DE-AC02-06CH11357.

- 
- [1] H. Timmers *et al.*, Nucl. Phys. A **633**, 421 (1998).
  - [2] B. B. Back, H. Esbensen, C. L. Jiang, and K. E. Rehm, Rev. Mod. Phys. **86**, 317 (2014).
  - [3] A. M. Stefanini *et al.*, Phys. Rev. C **76**, 014610 (2007).
  - [4] A. M. Stefanini *et al.*, Phys. Rev. C **73**, 034606 (2006).
  - [5] R. A. Broglia, C. H. Dasso, S. Landowne, and A. Winther, Phys. Rev. C **27**, 2433 (1983).

- [6] M. Beckerman *et al.*, Phys. Rev. Lett. **45**, 1472 (1980).
- [7] H. Esbensen and A. M. Stefanini, Phys. Rev. C **89**, 044616 (2014).
- [8] G. Montagnoli *et al.*, Eur. Phys. J. A **15**, 351 (2002).
- [9] S. Szilner *et al.*, Phys. Rev. C **76**, 024604 (2007).
- [10] L. Corradi *et al.*, Phys. Rev. C **84**, 034603 (2011).
- [11] Guillaume Scamps and Kouichi Hagino, Phys. Rev. C **92**, 054614 (2015).
- [12] V. V. Sargsyan, G. G. Adamian, N. V. Antonenko, W. Scheid, and H. Q. Zhang, Phys. Rev. C **85**, 024616 (2012).
- [13] A. M. Stefanini *et al.*, Phys. Lett. B **728**, 639 (2014).
- [14] R. A. Broglia and A. Winther, Frontiers in Physics Lecture Notes Series: Heavy-ion Reactions, Vol. 84 (Addison-Wesley, Redwood City, CA).
- [15] H. Esbensen and S. Landowne, Nucl. Phys. A **492**, 473 (1989).
- [16] H. Esbensen, C. L. Jiang and K. E. Rehm, Phys. Rev. C **57**, 2401 (1998).
- [17] J. M. Quesada, G. Pollarolo, R. A. Broglia, and A. Winther, Nucl. Phys. A **442**, 381 (1985).
- [18] K. E. Rehm *et al.*, Phys. Rev. C **42**, 2497 (1990).
- [19] C. H. Dasso and G. Pollarolo, Phys. Lett. **155B**, 223 (1985).
- [20] G. Pollarolo and A. Winther, Phys. Rev. C **62**, 054611 (2000).
- [21] N. Rowley, G. R. Satchler, and P. H. Stelson, Phys. Lett. B **254**, 25 (1991).
- [22] C. L. Jiang *et al.*, Phys. Rev. Lett. **89**, 052701 (2003).
- [23] H. Esbensen and C. L. Jiang, Phys. Rev. C **79**, 064619 (2009).

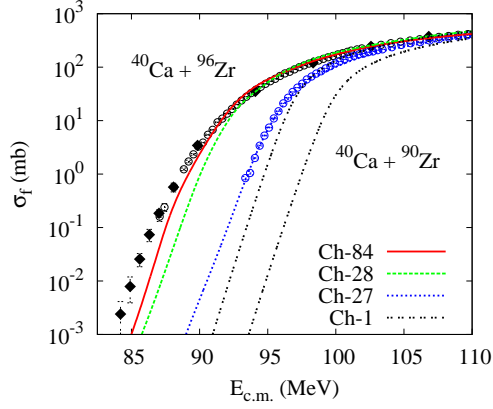


FIG. 1: (color online) Fusion cross sections for  $^{40}\text{Ca}+^{90,96}\text{Zr}$  [1]. The solid diamonds are the new data for  $^{40}\text{Ca}+^{96}\text{Zr}$  [13]. The curves are based on standard WS potentials. The Ch-1 calculations show the no-coupling limit for the two systems. The Ch-27 and Ch-28 calculations include couplings of up to three-phonon excitations. The Ch-84 calculation for  $^{40}\text{Ca}+^{96}\text{Zr}$  includes in addition couplings to one- and two-neutron transfer channels.

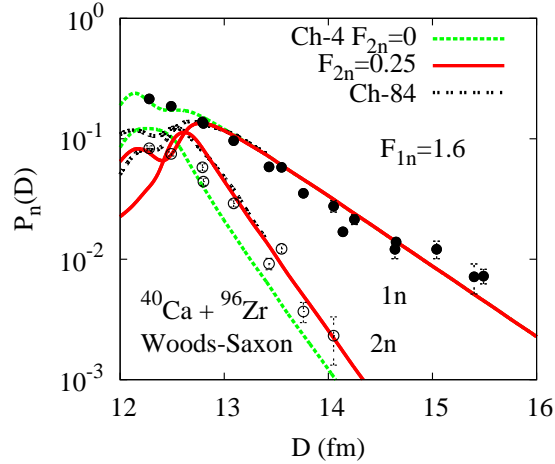


FIG. 2: (color online) Transfer probabilities for the one- and two-neutron transfer as functions of the distance of closest approach,  $D$ . The data are from Ref. [10]. All calculations use the one-neutron transfer strength  $F_{1n} = 1.6$ . The successive one-neutron transfer calculation (Ch-4 with  $F_{2n}=0$ ) reproduces the one-neutron transfer data at large values of  $D$  but it does not account for the two-neutron data. The solid curves include a direct pair transfer with strength  $F_{2n} = 0.25$  fm; it explains the two-neutron data quite well at large distances. The results of Ch-84 calculations are also shown.

TABLE I: Analysis of the  $^{40}\text{Ca}+^{96}\text{Zr}$  fusion data. The type of calculation is listed in the 1st column. All calculations use the same WS potential with  $R = 9.599$  fm,  $V_0 = -73.98$  MeV and diffuseness  $a = 0.673$  fm. The strengths of the one- and two-neutron transfer form factors are listed in the 2nd and 3rd column. The first  $\chi^2/N$  includes all data points. The  $\Delta E$  is the energy shift of the calculation that minimizes the  $\chi^2/N$  to the data, followed by the value of the minimum  $\chi^2/N$ . The analysis includes a systematic error of 7%.

Reaction	$F_{1n}$	$F_{2n}$ (fm)	$\chi^2/N$	$\Delta E$ (MeV)	$\chi^2/N$
Ch-84 old	1.0	0.5	4.10	-0.10	3.83
Ch-84 calibr.	1.6	0.25	6.70	-0.35	4.05
Ch-84 revised	2.25	0.355	0.87	-0.15	0.30
Ch-54	2.25	0.355	2.32	-0.08	2.14
Ch-72	2.25	0.355	1.80	-0.05	1.72
Ch-84	2.25	0.355	0.87	-0.15	0.30
Ch-112	2.25	0.355	1.13	-0.02	1.12

TABLE II: The one- and two-nucleon transfer cross sections (in mb) measured at 94.5 and 106 MeV [8] are compared to the results of the revised coupled-channels calculations that use the transfer strengths  $F_{1n} = 2.25$  and  $F_{2n} = 0.355$  fm.

Reaction	$E_{c.m.}$ (MeV)	$\sigma_{1N}$	$\sigma_{2N}$	$E_{c.m.}$ (MeV)	$\sigma_{1N}$	$\sigma_{2N}$
Ch-54	94.5	73	75	106.16	93	101
Ch-72	94.5	77	38	106.16	109	51
Ch-84	94.5	72	73	106.16	90	100
Ch-112	94.5	78	39	106.16	106	49
Ref. [8]	94.5	$75 \pm 10$	$16.5 \pm 2.1$	106.16	$117.9 \pm 8.5$	$56.9 \pm 4.6$

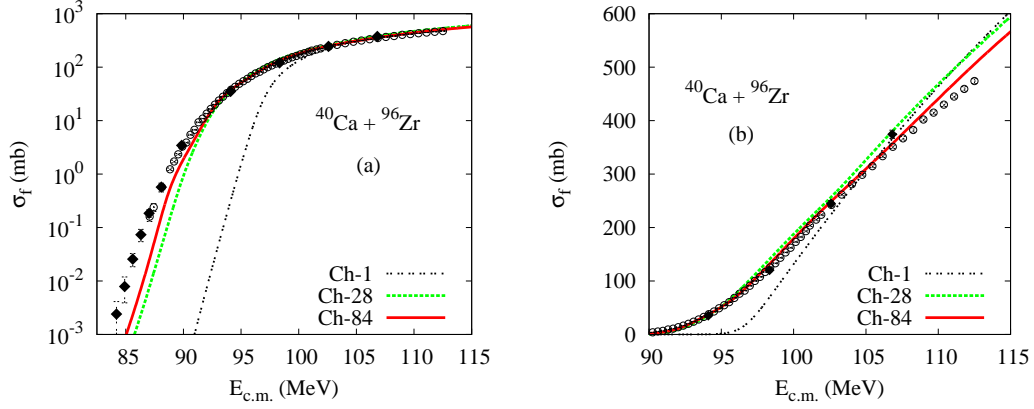


FIG. 3: (color online) Fusion cross sections for  $^{40}\text{Ca}+^{96}\text{Zr}$  [1, 13] are compared to coupled-channels calculations that are based on the same WS potential as used in Fig. 1. The Ch-1 calculation is the no-coupling limit. The Ch-28 calculation includes couplings of up to three-phonon excitations. The Ch-84 calculation (solid red curves) uses the transfer strengths  $F_{1n} = 1.6$  and  $F_{2n} = 0.25$  fm that were determined in Fig. 2.

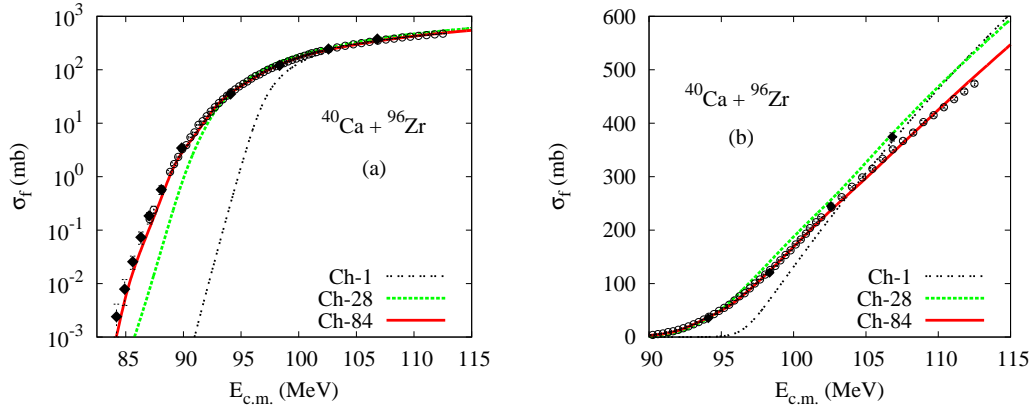


FIG. 4: (color online) Fusion cross sections for  $^{40}\text{Ca}+^{96}\text{Zr}$  [1, 13] are compared to the revised Ch-84 calculations where the transfer couplings have been multiplied by a  $\sqrt{2}$ . The results of the Ch-1 and Ch-28 calculations are the same as those shown in Fig. 3.

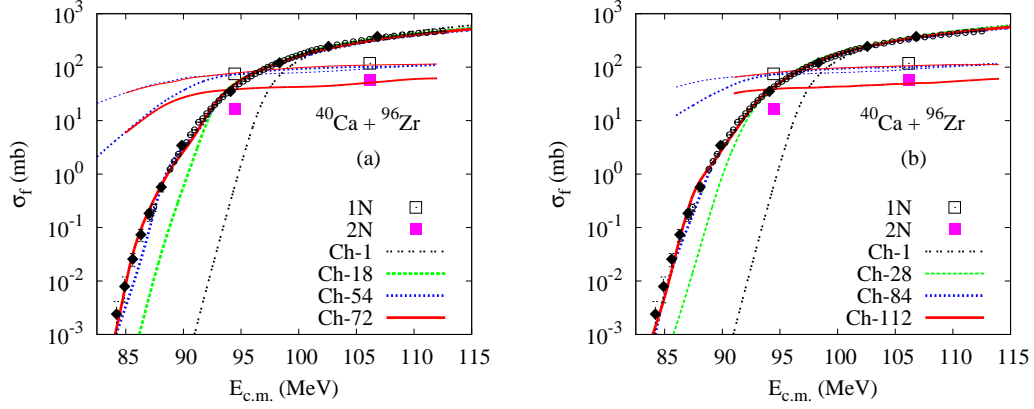


FIG. 5: (color online) Fusion cross sections for  $^{40}\text{Ca} + ^{96}\text{Zr}$  [1, 13] are compared to coupled-channels calculations that are based on (a) Ch-18 and (b) Ch-28 excitation channel calculations. The Ch-54 and Ch-84 calculations include up to two-nucleon transfers, and the Ch-72 and Ch-112 include up to three-nucleon transfers. The transfer strengths were set to  $F_{1n} = 2.25$  and  $F_{2n} = 0.355$  fm. The measured one-nucleon (1N) and two-nucleon (2N) cross sections [8] are compared to the calculations where the thin curves show the 1N and the thick curves the 2N cross sections.

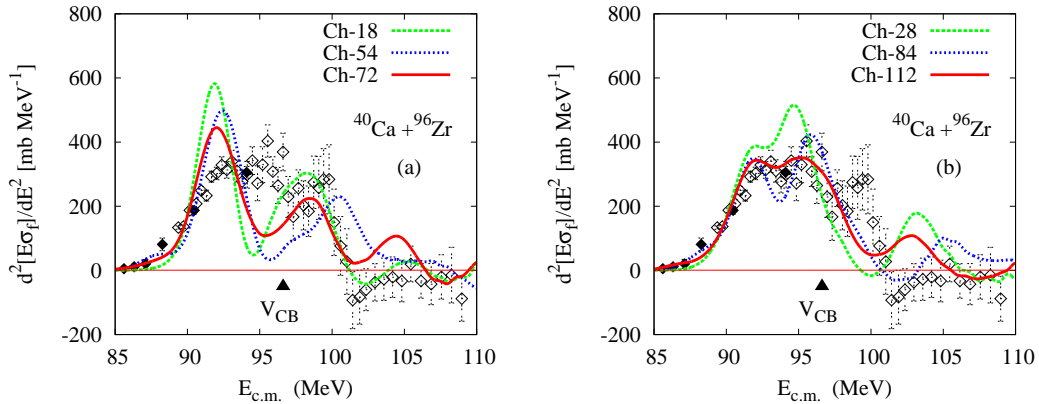


FIG. 6: (color online) Barrier distributions obtained from the fusion cross sections shown in Fig. 5.

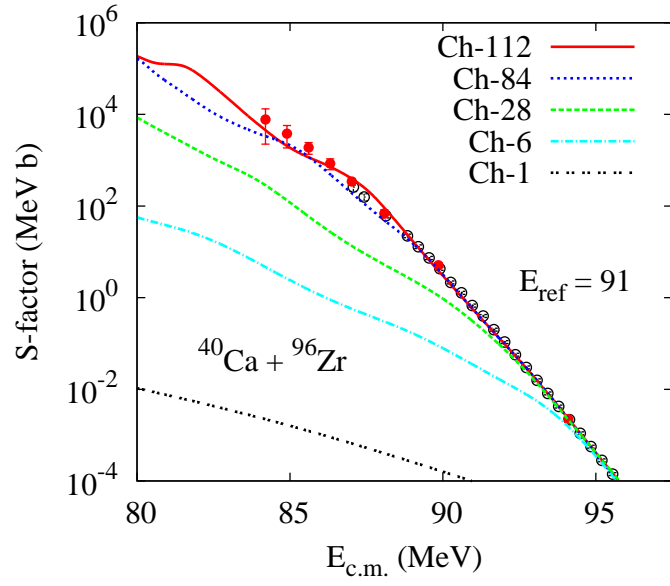


FIG. 7: (color online)  $S$  factors for the fusion cross sections shown in Fig. 5(b). The reference energy in Eq. (6) was set to  $E_{\text{ref}} = 91$  MeV. The second panel shows the results for a deeper WS (Adj WS) potential.